Engineering Journal issn: 0125-8281

Article

Effect of Thickness Eccentricity on the Stress Intensity Factors for a Pipe with a Single Internal Radial Crack under Internal Pressure

Jirapong Kasivitamnuay[1,a,*], Patchanida Seenuan[2,b], Nitikorn Noraphaiphipaksa[3,c], and Chaosuan Kanchanomai[2,d]

1 Department of Mechanical Engineering, Faculty of Engineering, Chulalongkorn University, Thailand
2 Department of Mechanical Engineering, Thammasat University, Thailand
3 Nitikorn Research Partner Co. Ltd., Thailand

E-mail: [a,*]jirapong.K@chula.ac.th (Corresponding author), [b]ingpatchanida@gmail.com, [c]nitikornrp@gmail.com, [d]kchao@engr.tu.ac.th

Abstract. The thickness eccentricity of a pipe occurs due to manufacturing limitations and may be exacerbated by service-induced degradation mechanisms. Fracture and remaining life assessments of a cracked eccentric pipe require a solution for the crack-tip parameters, e.g., the stress intensity factors (SIFs). However, the SIFs for this problem have not been examined. This study aimed to develop SIFs for an eccentric pipe with an infinitely longitudinal crack nucleated from an inner wall at the thinnest location of the pipe cross-section subjected to internal pressure. The problem was simplified to a cracked eccentric ring in a plane-strain condition, and finite element analysis was utilized for the determination of the SIFs, which were presented in tabulated form and empirical relation. The SIFs included a wide range of configuration parameters, i.e., a thin to thick-walled pipe, a shallow to deep crack, and a concentric pipe to a pipe with moderate thickness eccentricity. The need to consider the effect of eccentricity in SIFs calculation increased when the relative thickness of a pipe decreased and the relative crack depth increased.

Keywords: Finite element analysis, pipe, ring, stress intensity factor, thickness eccentricity.

ENGINEERING JOURNAL Volume 27 Issue 3
Received 12 September 2022
Accepted 13 March 2023
Published 31 March 2023
Online at https://engj.org/
DOI:10.4186/ej.2023.27.3.25

DOI:10.4186/ej.2023.27.3.25

1. Introduction

Pipes and pipelines are used extensively in the petrochemical, power, and offshore industries. Pipe manufacturers must control the geometrical imperfections of a pipe to satisfy product standards [1] since any imperfections can reduce the load-carrying capacity of a pipe. Two geometrical imperfections that are of significant concern in pipe strength calculations are ovality and thickness eccentricity. Ovality, or out-of-roundness, represents a deviation from a circular cross-section. Thickness eccentricity represents the non-uniform wall thickness of a pipe.

Even if the imperfections in an intact pipe meet the standard criteria, they may worsen during installation or servicing [2-4]. For a subsea pipeline, the influences of ovality and local wall thinning by corrosion on collapse pressure have been studied extensively [5-9]. Aside from subsea pipelines, the predominant load applied to the pipe is internal pressure meaning bursting is a prominent failure mode. For a pipe subjected to internal pressure, Huang et al. [10] reported that the thickness eccentricity had a critical influence on the pipe burst strength, while the effect of ovality was minor.

Because the shape of a worn or corroded area can be arbitrary, several geometrical representations of these damaged areas have been proposed, as shown in Fig. 1. Including a double circular arc (DCA), a groove, and a crescent-shaped, these are proposed as shown in Fig. 1. The advantage of DCA geometry is that it can represent the non-uniform wall thickness found in an intact pipe as well as servicing pipe with internal or external corrosion. Chen et al. [11] developed a burst pressure prediction equation based on DCA geometry. The equation successfully predicted the burst pressure for a pipe with thickness eccentricity due to internal wear [12] and internal corrosion [13-15]. Figure 2 depicts the capability of Chen's model in the prediction of the burst pressure for pipes made of medium and high-strength steel [15]. The plot suggests that the DCA geometry can model corroded pipe with a thickness eccentricity of up to 0.3 with an accuracy of ±15%.

Besides bursting, a pipe could be susceptible to cracking during service. The problem of cracking in a pipe with a non-uniform thickness could be found in two scenarios: crack-in-corrosion (CIC) [16-19], where a crack emanates from the bottom of a corroded area, and crack-in-erosion (CIE) [20, 21], where a crack emanates from an erosion groove. Studies have been conducted concerning a variety of shapes and locations for corrosion or erosion damage as well as crack types [16-21]. One of the main purposes of these studies was the development of solutions for stress intensity factors (SIFs) [18-21]. However, SIFs to analyze a crack in a corroded pipe with a pipe wall thickness represented by DCA geometry are unavailable.

Considering the internal pressure as a basic load case, a crack is prone to be oriented longitudinally due to the hoop stress. In addition, maximum hoop stress occurs at

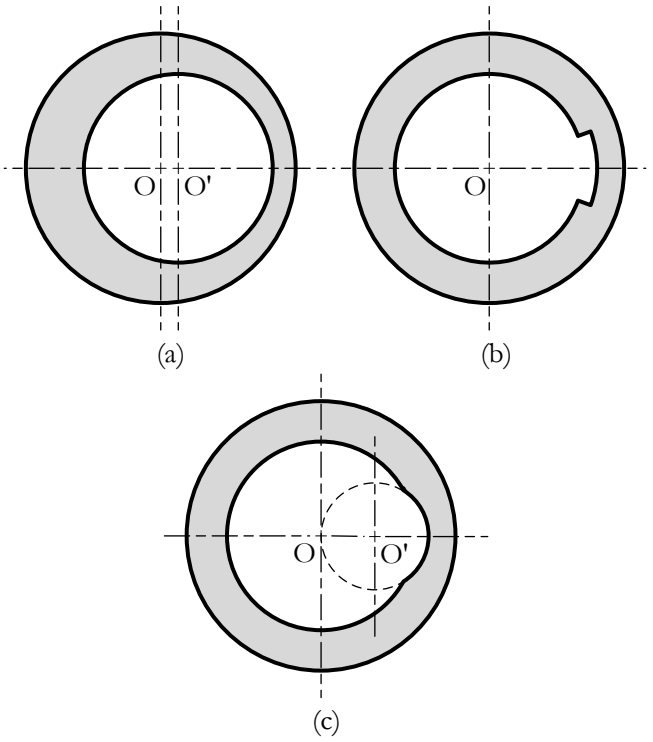

Fig. 1. Geometrical models for a pipe with a non-uniform thickness including (a) Double circular arc (DCA) model, (b) Groove model, and (c) Crescent-shaped model.

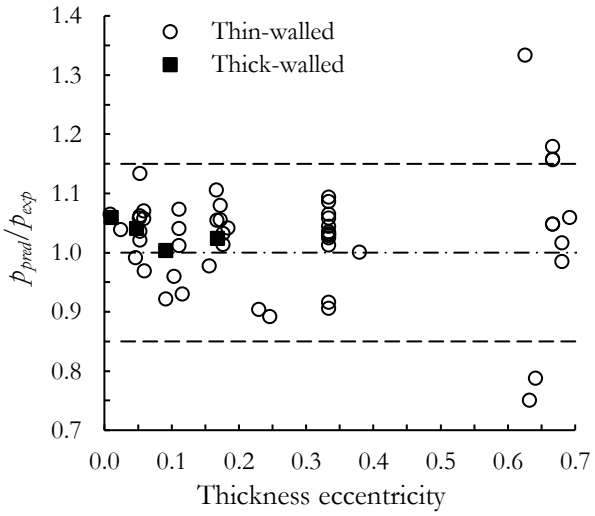

Fig. 2. Capability of the DCA geometry in the burst pressure prediction for a corroded pipe made of medium and high strength steels (Data from Ref. [15]; p_{pred} and p_{exp} denotes predicted and experimental burst pressures, respectively).

an inner wall of the thinnest location of a pipe cross-section [22]. Therefore, it is reasonable to assume that an inner-wall surface crack is likely to be nucleated from that location. Although the typically idealized shape of a surface crack assumed for a pipe is semi-elliptical [23], the crack-tip parameter calculation for this crack type is laborious. Kirkhope et al. [24] showed that the SIF for an internally pressurized concentric pipe with an infinitely

long crack was the upper limit of the SIF at the deepest point for an internally pressurized concentric pipe with a semi-elliptical surface crack. A similar trend was reported for a buried pipe [25]. These studies demonstrate a practical aspect of the SIF solution for this idealized crack shape (i.e., infinitely long crack) and the solution has been included in recognized fitness-for-service (FFS) standards [26].

This paper develops SIFs for a cracked pipe with a non-uniform thickness that can be represented by DCA geometry. The study concerns an infinitely long axial crack emanating from an inner wall at the thinnest location of a pipe cross-section in a pipe that is under internal pressure. The problem is simplified to an eccentric ring with an internal radial crack in a plane-strain condition. Two-dimensional FE analysis is employed to determine the SIFs. Validation of the results is demonstrated. The effect of thickness eccentricity on the SIF is discussed. The present SIFs could be utilized for predicting the critical pressure, critical crack size, and remaining life of a pipe with thickness eccentricity.

2. Finite Element Analysis

2.1. Geometry and Analyzed Cases

The geometry of an eccentric ring with an internal radial crack is shown in Fig. 3. The inner and outer walls of the ring have radii of R_i and R_o, respectively. The distance between the centers of the inner and outer walls is equal to δ. A crack with a depth of a is nucleated from the inner wall at the thinnest location of the ring. From this geometrical model, the maximum thickness t_{max} and the minimum thickness t_{min} of the pipe can be derived respectively as:

$$t_{max} = R_o - R_i + \delta \quad (1)$$

and

$$t_{min} = R_o - R_i - \delta, \quad (2)$$

Equations (1) and (2) are substituted into the definition of an average wall thickness t_{avg}, which is given by $(t_{max} + t_{min})/2$ yields:

$$t_{avg} = R_o - R_i \quad (3)$$

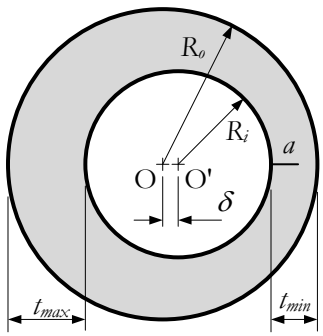

Fig. 3. Schematic representation of a cracked eccentric ring by DCA geometry.

The pipe thickness eccentricity e is defined as [11]:

$$e = \frac{t_{max} - t_{min}}{t_{max} + t_{min}} \quad (4)$$

Equations (1) and (2) are substituted into Eq. (4) and, using Eq. (3), the eccentricity can be rewritten as:

$$e = \frac{\delta}{t_{avg}} \quad (5)$$

Based on the dimensionless geometrical parameters for a cracked concentric ring (i.e., $\delta = 0$), which are t_{avg}/R_i and a/t_{avg} [26], the proposed dimensionless parameters for a cracked eccentric are t_{avg}/R_i, a/t_{min}, and e.

Table 1 summarizes the FE analysis cases. Six values of a relative thickness t_{avg}/R_i were chosen from 0.025 to 1, covering both thin-walled ($t_{avg}/R_i \leq 0.1$) and thick-walled ranges ($t_{avg}/R_i > 0.1$). The relative crack depth a/t_{min} ranged from 0.05 to 0.8. The eccentricity e varied from 0 (a concentric ring) to 0.30. This upper limit value of eccentricity was chosen because a fitness-for-service (FFS) assessment of a cracked component requires evaluation of both the fracture and the fully plastic yielding criterion. The DCA geometry could be used for an assessment of fully plastic yielding for a pipe with eccentricity up to 0.3, as shown in Fig. 1. As a result, the SIFs for FFS evaluation of a cracked eccentric pipe with eccentricity up to 0.3 were required. It should be noted that the eccentricity range studied covers the allowable eccentricity of an intact pipe (e = 0.125 [1]). However, it does not cover the eccentricity found in servicing pipe, which can reach 0.7 as shown in Fig. 2.

Table 1. Summary of FE analysis cases.

t_{avg}/R_i	a/t_{min}	e
0.025, 0.05, 0.1, 0.2, 0.5, 1	0.05, 0.1, 0.2, 0.4, 0.6, 0.8	0, 0.01, 0.02, 0.04, 0.06, 0.08, 0.10, 0.15, 0.20, 0.25, 0.30

2.2. Finite Element Model and Post-Processing

Due to symmetrical geometry and loading, only half of a cracked eccentric ring was modeled, as shown schematically in Fig. 4. On the symmetry line, the uncracked wall (i.e., line AB) and uncracked ligament (i.e., a line from crack tip to D) were restrained in the y-direction. Further, point A was restrained in the x-direction. Internal pressure p was applied at the inner wall and the crack surface.

For all analysis cases, the inner radius R_i and internal pressure p were set to 100 mm and 1 MPa, respectively. Additionally, the ring material was assumed to be isotropic linear elastic with Young's modulus and Poisson's ratio of 200 GPa and 0.3, respectively.

DOI:10.4186/ej.2023.27.3.25

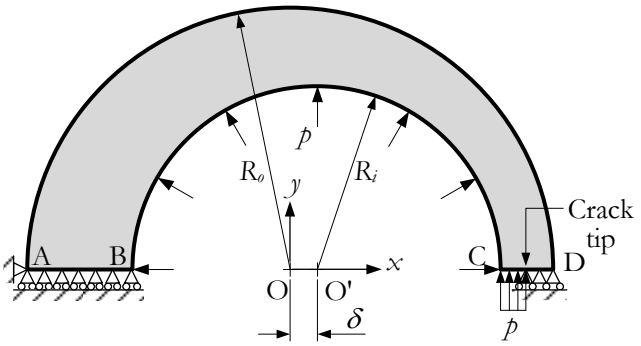

Fig. 4. Schematic representation of the FE model for a cracked eccentric ring.

ANSYS Mechanical APDL 2021 R1 was used in the FE modeling and analysis. A two-dimensional plane-strain linear elastic stress analysis was performed. The applied load was divided into 20 steps (from 0 to 1 MPa). The crack tip was encompassed with triangular quarter-point elements degenerated from an 8-node quadrilateral element (PLANE 183 element type in the software library). The remaining area of the ring was discretized using an 8-node quadrilateral element. The SIF was extracted from the FE solution using a displacement extrapolation technique via the KCALC command of the software.

Cracked concentric rings with t_{avg}/R_i = 0.5 and relative crack depth a/t_{avg} of 0.1 and 0.8 were selected as representative cases for determining proper mesh size, particularly at the crack tip, points C and D. Tables 2 and 3 show the effects of mesh size and the number of elements surrounding the crack tip on the SIFs. For all cases in the tables, mesh sizes at points C and D were set to $t_{avg}/100$ and $t_{avg}/10$ for a/t_{avg} of 0.1 but changed to $t_{avg}/10$ and $t_{avg}/100$ for a/t_{avg} of 0.8. A mesh with a size of $t_{avg}/100$ or finer and a number of surrounding elements of 10 or more resulted in SIFs with excellent convergence rates for both crack lengths. Tables 4 and 5 show the effects of mesh size at points C and D on the SIFs. According to the results, the mesh size of the point closest to the crack tip (point C for a/t_{avg} = 0.1 or point D for a/t_{avg} = 0.8) should be $t_{avg}/80$ or finer.

Finally, crack tip mesh size and the number of triangular quarter-point elements surrounding the crack tip for all analyzed cases were $t_{avg}/200$ and 12 elements, respectively. Element size at point C was set to either $t_{avg}/100$ for a/t_{min} = 0.05, 0.1, and 0.2 or $t_{avg}/10$ for a/t_{min} = 0.4, 0.6, and 0.8, whereas the element size at point D was set to either $t_{avg}/10$ for a/t_{min} = 0.05, 0.1, 0.2, 0.4, and 0.6 or $t_{avg}/100$ for a/t_{min} = 0.8. Figure 5 illustrates an example of the FE meshes for a cracked eccentric ring with t_{avg}/R_i = 0.5, a/t_{min} = 0.2 and e = 0.1. The number of nodes and elements used in this FE model were 4,574 and 1,443, respectively.

Table 2. Effect of crack tip mesh size on the SIFs for a cracked concentric ring with t_{avg}/R_i = 0.5.

Crack tip mesh size	a/t_{avg}			
	0.1		**0.8**	
	SIF ($MPa\sqrt{mm}$)	**Convergence rate (%)**	**SIF** ($MPa\sqrt{mm}$)	**Convergence rate (%)**
$t_{avg}/50$	16.170	-	94.220	-
$t_{avg}/100$	16.176	0.04	94.185	0.04
$t_{avg}/150$	16.162	0.09	94.090	0.10
$t_{avg}/200$	16.161	0.01	94.101	0.01
$t_{avg}/250$	16.153	0.05	94.065	0.04
$t_{avg}/300$	16.148	0.03	94.029	0.04

Table 3. Effect of the number of elements surrounding the crack tip on the SIFs for a cracked concentric ring with t_{avg}/R_i = 0.5.

No. of elements	a/t_{avg}			
	0.1		**0.8**	
	SIF ($MPa\sqrt{mm}$)	**Convergence rate (%)**	**SIF** ($MPa\sqrt{mm}$)	**Convergence rate (%)**
4	16.221	-	94.470	-
6	16.237	0.10	94.513	0.05
8	16.181	0.35	94.297	0.23
10	16.193	0.07	94.283	0.01
12	16.161	0.20	94.101	0.19
18	16.159	0.01	94.083	0.02

Table 4. Effect of mesh size of point C for a cracked concentric ring with $t_{avg}/R_i = 0.5$ and $a/t_{avg} = 0.1$.

Mesh size	SIF ($MPa\sqrt{mm}$)	Convergence rate (%)
$t_{avg}/10$	16.092	-
$t_{avg}/20$	16.151	0.37
$t_{avg}/40$	16.150	0.01
$t_{avg}/60$	16.166	0.10
$t_{avg}/80$	16.160	0.04
$t_{avg}/100$	16.161	0.01
$t_{avg}/120$	16.162	0.01

Table 5. Effect of mesh size of point D for a cracked concentric ring with $t_{avg}/R_i = 0.5$ and $a/t_{avg} = 0.8$.

Mesh size	SIF ($MPa\sqrt{mm}$)	Convergence rate (%)
$t_{avg}/10$	93.163	-
$t_{avg}/20$	93.942	0.83
$t_{avg}/40$	94.043	0.11
$t_{avg}/60$	94.080	0.04
$t_{avg}/80$	94.091	0.01
$t_{avg}/100$	94.101	0.01
$t_{avg}/120$	94.102	0.01

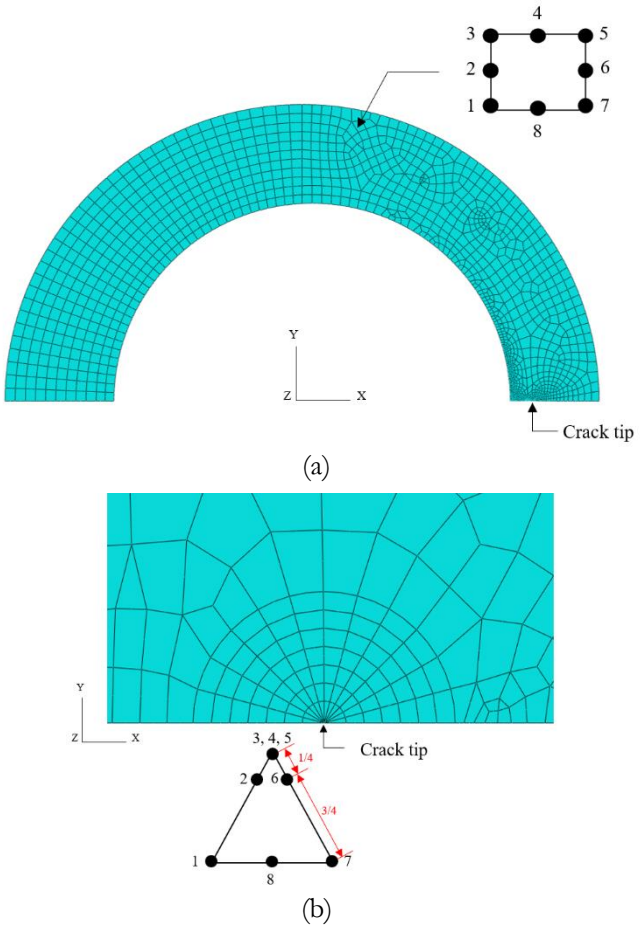

Fig. 5. Example of a FE mesh generated for the case of $t_{avg}/R_i = 0.5$, $a/t_{min} = 0.2$, and $e = 0.10$. (a) A half-model. (b) closed-up around the crack tip. Image courtesy of ANSYS, Inc.

2.3. Verification of the Finite Element Model

The validity of the FE model was confirmed by comparison with the SIF solution published in the API 579 code for the problem of a cracked concentric ring [26]. Most of the geometrical factors (also SIFs) for the present FE model conformed to the code solution as shown in Fig. 6. The deviations were less than 1.2% except for three cases including $t_{avg}/R_i = 0.5$ and $a/t_{avg} = 0.8$; and $t_{avg}/R_i = 1$ and $a/t_{avg} = 0.6$ and 0.8, where the deviations were 2.9%, 4.7%, and 13.7%, respectively. A mesh refinement was performed on these problematic cases. The convergence rates of SIFs were found to be less than 0.35%. Therefore, this research adopted the current FE solutions for these three cases. Moreover, the present FE models with previously specified element sizes were sufficient for application to the problem of a cracked eccentric ring.

3. The Stress Intensity Factor Solution

Based on the SIF solution for a cracked concentric ring [26], the following form of the mode-I SIF solution, K_I for a cracked eccentric ring was adopted.

$$K_I = \frac{pR_o^2}{R_o^2 - R_i^2}\sqrt{\pi a}\cdot F\left(\frac{t_{avg}}{R_i}, \frac{a}{t_{min}}, e\right) \quad (6)$$

where p is the internal pressure, a is the crack depth, R_i and R_o are the inner and outer radii, respectively, t_{avg} is the nominal thickness, and F is a geometrical factor that is dependent on the chosen dimensionless parameters, i.e., t_{avg}/R_i, a/t_{min}, and e. By substituting the SIF obtained from the FE analysis and the relevant dimensional variables into Eq. (6), the geometrical factor F can be determined. The values of F for all analysis cases are tabulated in Table 6.

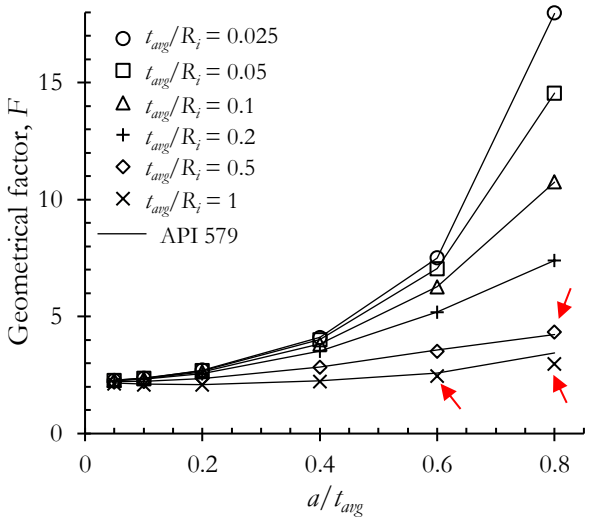

Fig. 6. Verification of the present FE results with the API 579 solution for a cracked concentric ring. Cases of significant deviation are indicated by red arrows.

Table 6. Values of the geometrical factor *F* for a ring with a single internal radial crack under internal pressure.

e	a/t_{min}	t_{avg}/R_i					
		0.025	**0.05**	**0.1**	**0.2**	**0.5**	**1**
0	0.05	2.277	2.273	2.266	2.250	2.205	2.137
	0.1	2.372	2.364	2.347	2.314	2.225	2.091
	0.2	2.715	2.694	2.652	2.571	2.360	2.087
	0.4	4.116	4.020	3.841	3.528	2.850	2.221
	0.6	7.518	7.051	6.284	5.187	3.529	2.474
	0.8	17.983	14.567	10.778	7.414	4.354	2.974
0.01	0.05	2.298	2.295	2.286	2.267	2.217	2.144
	0.1	2.395	2.386	2.368	2.332	2.237	2.099
	0.2	2.741	2.719	2.676	2.591	2.374	2.096
	0.4	4.157	4.059	3.877	3.557	2.869	2.232
	0.6	7.592	7.121	6.339	5.232	3.554	2.490
	0.8	18.161	14.709	10.880	7.480	4.387	2.992
0.02	0.05	2.321	2.317	2.306	2.285	2.229	2.151
	0.1	2.418	2.409	2.389	2.350	2.250	2.107
	0.2	2.768	2.745	2.700	2.612	2.388	2.105
	0.4	4.198	4.098	3.913	3.586	2.887	2.243
	0.6	7.667	7.189	6.399	5.277	3.579	2.503
	0.8	18.343	14.854	10.985	7.547	4.420	3.010
0.04	0.05	2.369	2.362	2.348	2.321	2.254	2.166
	0.1	2.470	2.456	2.433	2.389	2.276	2.124
	0.2	2.824	2.799	2.749	2.655	2.418	2.124
	0.4	4.283	4.179	3.986	3.648	2.928	2.267
	0.6	7.824	7.332	6.522	5.373	3.632	2.532
	0.8	18.720	15.155	11.202	7.689	4.491	3.048
0.06	0.05	2.418	2.409	2.392	2.358	2.280	2.182
	0.1	2.518	2.505	2.479	2.428	2.303	2.141
	0.2	2.883	2.855	2.802	2.701	2.448	2.145
	0.4	4.372	4.264	4.063	3.712	2.969	2.292
	0.6	7.987	7.483	6.648	5.473	3.689	2.562
	0.8	19.115	15.471	11.430	7.838	4.565	3.088
0.08	0.05	2.468	2.457	2.437	2.398	2.308	2.198
	0.1	2.571	2.556	2.526	2.470	2.331	2.158
	0.2	2.944	2.914	2.855	2.748	2.482	2.165
	0.4	4.465	4.352	4.142	3.780	3.016	2.323
	0.6	8.156	7.639	6.785	5.573	3.744	2.591
	0.8	19.528	15.804	11.670	7.995	4.643	3.130
0.10	0.05	2.521	2.508	2.484	2.439	2.336	2.216
	0.1	2.626	2.609	2.576	2.513	2.361	2.177
	0.2	3.007	2.975	2.912	2.797	2.515	2.187
	0.4	4.562	4.444	4.225	3.850	3.062	2.351
	0.6	8.334	7.801	6.926	5.684	3.809	2.629
	0.8	19.963	16.153	11.917	8.160	4.726	3.174
0.15	0.05	2.664	2.647	2.613	2.552	2.412	2.261
	0.1	2.776	2.754	2.710	2.630	2.442	2.228
	0.2	3.179	3.141	3.065	2.930	2.608	2.246
	0.4	4.824	4.696	4.457	4.044	3.183	2.423
	0.6	8.811	8.240	7.305	5.980	3.981	2.722
	0.8	21.145	17.109	12.612	8.614	4.953	3.296
0.20	0.05	2.825	2.802	2.758	2.679	2.498	2.314
	0.1	2.945	2.916	2.862	2.762	2.533	2.285
	0.2	3.372	3.327	3.238	3.080	2.712	2.313
	0.4	5.122	4.979	4.710	4.257	3.321	2.511
	0.6	9.353	8.743	7.739	6.321	4.178	2.831
	0.8	22.490	18.201	13.409	9.142	5.214	3.434

Table 6. (Cont'd) Values of the geometrical factor F for a ring with a single internal radial crack under internal pressure.

e	a/t_{min}	t_{avg}/R_i					
		0.025	**0.05**	**0.1**	**0.2**	**0.5**	**1**
0.25	0.05	3.008	2.979	2.923	2.820	2.596	2.370
	0.1	3.136	3.100	3.033	2.910	2.636	2.349
	0.2	3.592	3.539	3.434	3.249	2.830	2.388
	0.4	5.453	5.294	5.003	4.506	3.491	2.613
	0.6	9.969	9.314	8.236	6.708	4.399	2.960
	0.8	24.031	19.458	14.331	9.747	5.515	3.593
0.30	0.05	3.219	3.182	3.110	2.984	2.707	2.439
	0.1	3.354	3.311	3.228	3.081	2.754	2.423
	0.2	3.843	3.780	3.659	3.448	2.965	2.475
	0.4	5.834	5.658	5.338	4.794	3.678	2.728
	0.6	10.678	9.972	8.814	7.161	4.659	3.088
	0.8	25.807	20.915	15.403	10.457	5.868	3.779

To facilitate the fracture assessment and the remaining life prediction, it is beneficial to express the geometrical factor by using a closed-form equation. The appropriate expression was developed using a systematic trial-error approach. First, the F values at specific a/t_{min} and various t_{avg}/R_i ratios were plotted against e, as shown in Fig. 7(a). It was found that the second-order polynomial function fitted the plots very well for all t_{avg}/R_i ratios. Next, the polynomial coefficients of the second-order, first-order, and zeroth-order terms at specific t_{avg}/R_i were plotted against a/t_{min} as shown in Fig. 7(b). It was found that the coefficients of the same order terms correlated with a/t_{min} by the fourth-order polynomial function. Lastly, the polynomial coefficients of the second-order, first-order, and zeroth-order terms at specific a/t_{min} were plotted against $\ln(t_{avg}/R_i)$, as shown in Fig. 7(c). It was found that the third-order polynomial function fitted the plots accurately.

From a systematic observation of the variation of F on the parameters t_{avg}/R_i, a/t_{min}, and e, the following empirical equation for the geometrical factor F was proposed.

$$F = \sum_{k=0}^{2}\sum_{j=0}^{3}\sum_{i=0}^{4} M_{ijk} \cdot \left(\frac{a}{t_{min}}\right)^i \cdot \left[\ln\left(\frac{t_{avg}}{R_i}\right)\right]^j \cdot e^k \qquad (7)$$

This equation can be used to determine the geometrical factor for a cracked concentric ring by replacing a/t_{min} with a/t_{avg} (since both parameters are equivalent for concentric case) and substituting $e = 0$.

Non-linear regression with the aid of MathCAD Prime 4 software was applied to the F values in Table 6. The best-fit coefficients M_{ijk} are listed in Table 7. A total of 86% of the deviations for the closed-form values from the FE results in Table 6 were within 1%, while all predictions were within 3.1%. The sixty coefficients M_{ijk} could be implemented into a computer code that allows the program to directly calculate the SIFs for any cracked eccentric ring. Consequently, the program becomes simpler and faster since it is not necessary to manipulate a large-size array variable which stores the tabulated F values for interpolation. An increase in calculation speed is noticeable in the case of a crack growth analysis where it is necessary to calculate the SIFs repeatedly.

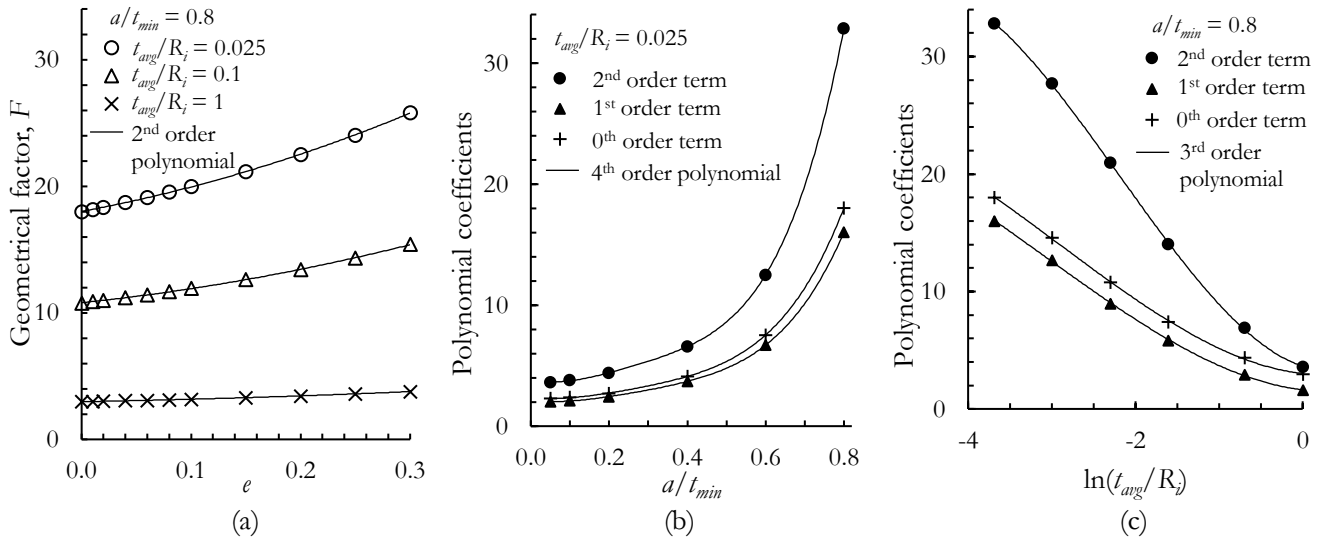

Fig. 7. A systematic plot to find basis functions for forming an empirical equation (Eq. (7)).

The empirical equation for SIFs (Eqs. (6) and (7)) was applied to six additional cracked eccentric pipes having different dimensions and Young's modulus from those listed in Section 2.2. For all cases, the inner radius R_i and internal pressure p were set to 50 mm and 1 MPa, respectively. The material properties of a pipe were assumed to be linear elastic with Young's modulus of 207 GPa, and Poisson's ratio of 0.3. The values of t_{avg}/R_i, a/t_{min}, and e for each case are listed respectively in columns 2-4 of Table 8. FE analyses were carried out and the SIFs were compared with those determined from the empirical equation as shown in Table 8. The F values for calculating the SIFs from the empirical equation were obtained either from Table 6 or Eq. (7). All results were in good agreement. The maximum difference was less than 0.6%. Accordingly, the empirical equation for SIF calculation for an eccentric pipe was confirmed.

Table 7. Coefficients M_{ijk} in empirical equation for the geometrical factor F (Eq. (7)).

k	i	j			
		0	**1**	**2**	**3**
0	0	2.2148	0.0031	-0.0174	-0.0087
	1	-1.9680	-2.5417	-0.2763	0.1580
	2	9.0554	2.9413	-2.7179	-1.7035
	3	-13.9425	-14.7220	5.8089	4.4865
	4	9.0959	16.9207	1.3737	-2.7976
1	0	0.5788	-0.8683	-0.2191	-0.0273
	1	1.3773	3.2474	2.7222	0.6258
	2	-0.9049	-14.7485	-12.4810	-3.2967
	3	-0.0571	15.1798	21.7085	6.9442
	4	1.3745	-2.1311	-9.0086	-4.3173
2	0	1.1190	-0.7999	0.1873	0.0551
	1	-0.1442	-9.9300	-6.6262	-0.9157
	2	17.3114	53.8905	35.3024	4.2334
	3	-36.9801	-135.1406	-78.4000	-7.8115
	4	25.5518	100.3569	63.8231	6.1041

Table 8. Comparison of the SIFs determined by the empirical equations (Eqs. (6) and (7)) with the FE results for eccentric cracked pipes with an inner radius R_i of 50 mm.

Case	t_{avg}/R_i	a/t_{min}	e	K_I (MPa$\sqrt{\text{m}}$)			% Difference	
				FEA	F **from Table 6**	F **by Eq. (7)**	F **from Table 6**	F **by Eq. (7)**
1	0.025	0.4	0.01	3.4071	3.4020	3.3912	0.15	0.47
2	0.025	0.4	0.20	3.7716	3.7681	3.7568	0.09	0.39
3	0.1	0.4	0.01	1.7647	1.7619	1.7616	0.16	0.18
4	0.1	0.4	0.20	1.9289	1.9241	1.9250	0.25	0.20
5	1	0.4	0.01	0.7449	0.7422	0.7407	0.36	0.56
6	1	0.4	0.20	0.7529	0.7506	0.7488	0.30	0.54

4. Discussion

The need for involving eccentricity in the SIFs calculation can be understood by comparing the geometrical factors for cracked concentric and eccentric rings with the same t_{avg}/R_i and crack length a. The relative crack depth in a cracked concentric ring a/t_{avg} is related to the relative crack depth in a cracked eccentric ring a/t_{min} by the following relationship:

$$\frac{a}{t_{avg}} = (1-e)\frac{a}{t_{min}} \tag{8}$$

Let the geometrical factors for cracked concentric and eccentric rings (same t_{avg}/R_i and a) be denoted as F_0 and F, respectively. Figure 8 conceptually depicts the meaning of F_0 and F of the cracked rings with the same crack length. Thus, the ratio F/F_0 represents the effect of eccentricity on the SIFs when compared to those that neglected it. Figure 9 shows the trends of F/F_0 versus a/t_{min} for cracked eccentric rings with t_{avg}/R_i = 0.025 and 1, and e = 0.1 and 0.2. The F/F_0 ratios are higher than unity which indicates that the SIFs are always higher for a cracked eccentric ring than those for a cracked concentric ring having equal t_{avg}/R_i and a/t_{min}. For the same value of t_{avg}/R_i, F/F_0 for e = 0.2 is higher than that for e = 0.1 for any values of a/t_{min}. In addition, F/F_0 is more sensitive to a/t_{min} for higher eccentricity. For higher t_{avg}/R_i, however, the significance of including eccentricity in the SIF calculation and the sensitivity to a/t_{min} is lower. In other words, the SIFs of a thin-walled pipe are more sensitive to eccentricity than a thick-walled pipe.

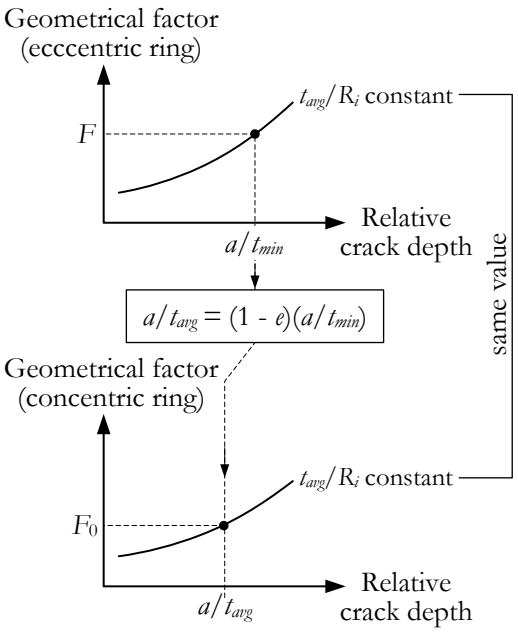

Fig. 8. Concept for comparing the geometrical factors of a cracked eccentric ring F with a concentric ring F_0 that has the same t_{avg}/R_i and crack length a.

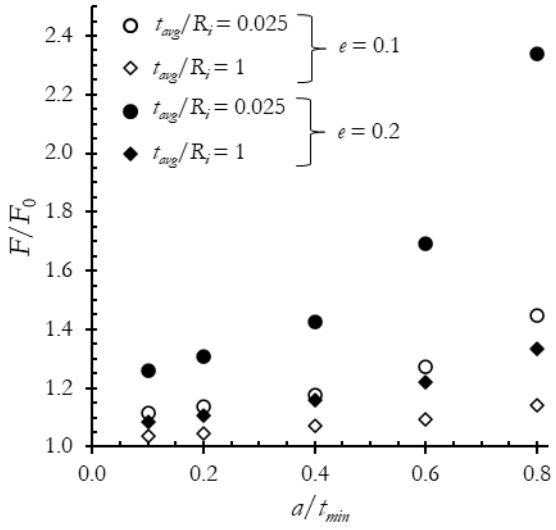

Fig. 9. Dependence of F/F_0 on the relative crack depth a/t_{min} for different eccentricities e and relative thickness t_{avg}/R_i of a cracked ring.

The effect of eccentricity on the SIF manifested the necessity for a measurement of a pipe thickness profile during an inspection in addition to a measurement of crack size. Furthermore, thickness eccentricity should be determined from the measured profile and incorporated into the calculation of the SIF to improve the fracture and remaining life analyses.

When considering an intact pipe, standard specification for a steel pipe, e.g., the ASTM standard [1], specify that the permissible variation of the minimum thickness from a nominal (average) thickness should be within 12.5%. This permissible limit is equivalent to the thickness eccentricity of 0.125. The F/F_0 ratios for this eccentricity at different t_{avg}/R_i, and a/t_{min} were linear interpolated from F/F_0 at e = 0.1 and e = 0.15. The results are summarized in Table 9. If a crack with a relative crack depth of 5% is nucleated in an eccentric ring, the F factor (also SIF) will increase 13.4% for t_{avg}/R_i = 0.025 but will decrease continually to 4.3% for t_{avg}/R_i = 1. From a fracture mechanics standpoint, the results support the importance of improving manufacturing processes to control or reduce the thickness eccentricity of a pipe, especially for a thin-walled pipe. Yet previous studies [24, 25] have shown that the influence of eccentricity on the SIFs might be lower in the case of a semi-elliptical surface crack with a low aspect ratio. Therefore, a permissible limit for the minimum thickness variation specified in the standard was reasonable. Future studies are still required to evaluate the influence of eccentricity on SIFs for the other crack and load configurations in a pipe.

Table 9. F/F_0 ratio of a pipe with minimum thickness variation at a permissible limit (e = 0.125).

a/t_{min}	t_{avg}/R_i					
	0.025	**0.05**	**0.1**	**0.2**	**0.5**	**1**
0.050	1.134	1.134	1.126	1.110	1.077	1.043
0.1	1.147	1.145	1.135	1.118	1.084	1.048
0.2	1.189	1.180	1.164	1.143	1.105	1.063
0.4	1.268	1.271	1.253	1.219	1.156	1.094
0.6	1.483	1.432	1.370	1.298	1.192	1.130
0.8	1.802	1.643	1.498	1.356	1.197	1.227

5. Conclusions

Commercial FE software (ANSYS) was utilized to determine the SIFs for an eccentric ring with a single radial crack at an inner wall and subjected to internal pressure. The accuracy of the FE models was confirmed with the solution from the API 579 code for the case of a cracked concentric ring. The maximum difference was less than 1.2%. The geometrical factors for both cracked concentric (36 cases) and eccentric rings (360 cases) derived from the FE analysis covered thin to thick-walled rings (i.e., $0.025 \le t_{avg}/R_i \le 1$), shallow to deep cracks (i.e., $0.05 \le a/t_{min} \le 0.8$), and nil to moderate eccentricity, (i.e., $0 \le e \le 0.3$). The results are presented in tabulated form and empirical relation. The accuracy of the empirical relation is better than 3.1% within the studied ranges of geometrical parameters (i.e., $0.025 \le t_{avg}/R_i \le 1$, $0.05 \le a/t_{min} \le 0.8$, a/t_{min}, and $0 \le e \le 0.3$).

The need to consider the effect of eccentricity in the SIFs calculation increased as t_{avg}/R_i decreased or a/t_{min} increased. For an intact pipe, the specified permissible thickness variation in the ASTM standard [1] was quantitatively evaluated based on the fracture mechanics concept and found to be appropriate. The importance of controlling the thickness eccentricity from manufacture and acquiring the wall thickness profile of a pipe in service was emphasized.

Acknowledgments

This research did not receive any specific grant from funding agencies in the public, commercial, or not-for-profit sectors.

References

[1] ASTM, "ASTM A530/A530M-18 Standard specification for general requirements for specialized carbon and alloy steel pipe," in *ASTM Vol. 01.01: Steel–Piping, Tubing, Fitting*. PA, USA: ASTM International, 2018.

[2] S. Kyriakides and E. Corona, *Mechanics of Offshore Pipelines Vol. 1: Buckling and Collapse*. Elsevier, 2007.

[3] W. H. Ahmed, "Evaluation of the proximity effect on flow-accelerated corrosion," *Ann. Nucl. Energy*, vol. 37, pp. 598-605, 2010.

[4] Q. Zhang, Z. Lian, and T. Lin, "Prediction of residual burst strength of worn casing by theoretical and numerical modelling," *Int. J. Pres. Ves. Pip.*, vol. 188, p. 104195, 2020.

[5] J. H. Baek, Y. P. Kim, and W. S. Kim, "Effect of thickness eccentricity on plastic collapse of subsea pipeline under external pressure," *J. Korean Inst. Gas.*, vol. 15, pp. 14-19, 2011.

[6] X. Zhang and G. Pan, "Collapse of thick-walled subsea pipelines with imperfections subjected to external pressure," *Ocean Eng.*, vol. 213, p. 107705, 2020.

[7] T. He, M. Duan, and C. An, "Prediction of the collapse pressure for thick-walled pipes under external pressure," *Appl. Ocean Res.*, vol. 47, pp. 199-203, 2014.

[8] H. Ye, S. Yan, and Z. Jin, "Collapse of corroded pipelines under combined tension and external pressure," *PLoS ONE*, vol. 11, p. e0154314, 2016.

[9] X. Zhang, B. Chen, and C. G. Soares, "Effect of non-symmetrical corrosion imperfection on the collapse pressure of subsea pipelines," *Mar. Struct.*, vol. 73, p. 102806, 2020.

[10] X. Huang, Y. Chen, K. Lin, M. Mihsein, K. Kibble, and R. Hall, "Burst strength analysis of casing with geometrical imperfections," *J. Press. Vess.-T. ASME.*, vol. 129, p. 763770, 2007.

[11] Z. Chen, W. Zhu, Q. Di, and W. Wang, "Prediction of burst pressure of pipes with geometric eccentricity," *J. Press. Vess.-T. ASME.*, vol. 137, p. 061201, 2015.

[12] Z. Chen, W. Zhu, Q. Di, and S. Li, "Numerical and theoretical analysis of burst pressures for casings with eccentric wear," *J. Petrol. Sci. Eng.*, vol. 145, pp. 585-591, 2016.

[13] Z. Chen, S. Yan, H. Ye, Z. Deng, X. Shen, and Z. Jin, "Double circular arc model based on average shear stress yield criterion and its application in the corroded pipe burst," *J. Petrol. Sci. Eng.*, vol. 149, pp. 515-521, 2017.

[14] Z. Chen, S. Yan, H. Ye, X. Shen, and Z. Jin, "Effect of the Y/T on the burst pressure for corroded pipelines with high strength," *J. Petrol. Sci. Eng.*, vol. 157, pp. 760-766, 2017.

[15] U. Bhardwaj, A. P. Teixeira, C. G. Soares, M. S. Azad, W. Punurai, and P. Asavadorndeja, "Reliability assessment of thick high strength pipelines with corrosion defect," *Int. J. Pres. Ves. Pip.*, vol. 177, p. 103982, 2019.

[16] B. Bedairi, D. Cronin, A. Hosseini, and A. Plumtree, "Failure prediction for crack-in-corrosion defects in natural gas transmission pipelines," *Int. J. Pres. Ves. Pip.*, vol. 96-97, pp. 90-99, 2012.

[17] B. C. Mondal and A. S. Dhar, "Burst pressure assessment of corroded pipelines using fracture mechanics criterion," *Eng. Fail. Anal.*, vol. 104, pp. 139-153, 2019.

[18] A. H. Akhi and A. S. Dhar, "Stress intensity factors for external corrosions and cracking of buried cast iron pipes," *Eng. Frac. Mech.*, vol. 250, p. 107778, 2021.

[19] A. H. Akhi and A. S. Dhar, "Fracture parameters for buried cast iron pipes subjected to internal surface corrosions and cracks," *J. Pipeline Sci. Eng.*, vol. 1, pp. 187-197, 2021.

[20] A. A. Becker, R. C. A. Plant, and A. P. Parker, "Axial cracks in pressurised eroded autofrettaged thick cylinders," *Int. J. Fracture.*, vol. 63, pp. 113-134, 1993.

[21] M. Perl, C. Levy, and J. Bu, "Three-dimensional analysis of a semi-elliptical crack emanating from an erosion at the bore of an autofrettaged pressurized cylinder," *J. Press. Vess.-T. ASME.*, vol. 121, pp. 209–215, 1999.

[22] S. P. Timoshenko, and J. N. Goodier, *Theory of Elasticity*, 3rd ed. Singapore: McGraw-Hill, 1970.

[23] J. C. Newman, and I. S. Raju, "Stress intensity factors for internal surface cracks in cylindrical pressure vessels," *J. Press. Vess.-T. ASME.*, vol. 102, pp. 342-346, 1980.

[24] K. J. Kirkhope, R. Bell, and J. Kirkhope, "Stress intensity factors for single and multiple semi-elliptical surface cracks in pressurized thick-walled cylinders," *Int. J. Pres. Ves. Pip.*, vol. 47, pp. 247-257, 1991.

[25] M. R. Ayatollahi, and H. Khoramishad, "Stress intensity factors for an axially oriented internal crack embedded in a buried pipe," *Int. J. Pres. Ves. Pip.*, vol. 87, pp. 165-169, 2010.

[26] American Petroleum Institute, *API 579-1/ASME FFS-1 Fitness-For-Service*. NY, USA: American Society of Mechanical Engineers, 2016.

Jirapong Kasivitamnuay received his B. Eng. and M. Eng. degrees from Chulalongkorn University, and doctoral degree in mechanical engineering from The University of Tokyo. Since 2000, he has been a faculty member at the Department of Mechanical Engineering, Chulalongkorn University. At present, he is an associate professor. His research interest is fracture mechanics, fatigue, and development of a classroom demonstration rigs for the mechanics of materials course.

Patchanida Seenuan was born in Phitsanulok, Thailand is 1997. She received the B.Eng. in mechanical engineering from Thammasat University, Pathum Thani in 2019 and the M.Eng. in mechanical engineering from Thammasat University, Pathum Thani in 2021.

At present, she is studying the Ph.D. in mechanical engineering of Thammasat University, Thailand. Her research interests include experimental, fracture mechanics and finite element analysis

Nitikorn Noraphaiphipaksa received the B.Eng. in mechanical engineering from Thammasat University, Pathum Thani in 2008, the M.Eng. in mechanical engineering from Thammasat University, Pathum Thani in 2011, and the Ph.D. in mechanical engineering, from Thammasat University, Pathum Thani in 2015.

At present, he is a research assistant with the Thammasat University and founder and CEO of Nitikorn Research Partner Co., Ltd., Thailand. He is the author of more than 15 articles with impact factor. His research interests include fatigue, failure, fracture mechanics, materials, mechanical design and finite element analysis.

Chaosuan Kanchanomai was born in Bangkok, Thailand is 1970. He received the B.Eng. in industrial engineering from Kasetsart University, Bangkok in 1991, the M.S. in mechanical engineering from the University of Southern California, Los Angeles, CA, in 1995, and the D.Eng. in materials science from Nagaoka University of Technology, Japan, in 2002.

From 1991 to present, he was a lecturer with the Thammasat University, Thailand. Since 2015, he has been a Full Professor with the Department of Mechanical Engineering. He is the author of more than 50 articles with impact factor. His research interests include experimental and computational fracture mechanics, low cycle fatigue, high cycle fatigue, fatigue crack growth, creep crack growth, fretting fatigue, and wear.